DOE-NP SBIR Phase II Project DE-SC0007520
Phase II Final Technical Report

Commercial Superconducting Electron Linac for Radioisotope Production

Terry L. Grimm, Chase H. Boulware, Jerry L. Hollister, Randall W. Jecks II, Mayir Mamtimin and Valeriia Starovoitova,
Niowave, Inc.
Lansing, MI 48906

Collaborators
Idaho State University / Idaho Accelerator Center

INTRODUCTION

The majority of radioisotopes used in the United States today come from foreign suppliers or are generated parasitically in large government accelerators and nuclear reactors. Both of these restrictions limit the availability of radioisotopes and discourage the development and evaluation of new isotopes and for nuclear medicine, science, and industry. Numerous studies have been recommending development of dedicated accelerators for production of radioisotopes for over 20 years (Institute of Medicine, 1995; Reba, et al, 2000; National Research Council, 2007; NSAC 2009). The 2015 NSAC Long Range Plan for Isotopes again identified electron accelerators as an area for continued research and development [1]. Recommendation 1(c) from the 2015 NSAC Isotope report specifically identifies electron accelerators for continued funding for the purpose of producing medical and industrial radioisotopes. Recognizing the pressing need for new production methods of radioisotopes, the United States Congress passed the American Medical Isotope Production Act of 2012 to develop a domestic production of ^{99}Mo and to eliminate the use of highly enriched uranium (HEU) in the production of ^{99}Mo [2].

One of the advantages of high power electron linear accelerators (linacs) is they can create both proton- and neutron-rich isotopes by generating high energy x-rays that knock out protons or neutrons from stable atoms or by fission of uranium. This allows for production of isotopes not possible in nuclear reactors. Recent advances in superconducting electron linacs have decreased the size and complexity of these systems such that they are economically competitive with nuclear reactors and large, high energy accelerators. Niowave, Inc. has been developing a radioisotope production facility based on a superconducting electron linac with liquid metal converters.

This project was supported by DOE Nuclear Physics under grant DE-SC0007520

EXECUTIVE SUMMARY

During the course of this Phase II of this project, Niowave has made significant progress towards operating a radioisotope production facility using a superconducting electron linac with multiple liquid metal converters. A 40 MeV, 100 kW superconducting electron linac has been designed and the research and development path for the hardware has been started, involving 10 MeV and 20 MeV SRF linacs. We have also designed and prototyped liquid metal converter/target units to investigate both photonuclear and neutron capture production routes. Niowave has estimated radioisotope production yields and benchmarked these simulations using a 40 MeV linac at the Idaho Accelerator Center. A dedicated radioisotope production facility has been designed, and the first building has been built in Lansing, MI, near the Capital Region International Airport. We have received approval of our shielding plan for electron beams up to 40 MeV and 100 kW at the Airport Facility from the State of Michigan's department of Licensing and Regulatory Affairs (LARA) radiation safety section. Niowave is licensed from the Nuclear Regulatory Commission (NRC) to produce isotopes both from stable targets and from uranium (natural, depleted, and low-enriched). Finally, we have established partnership with several isotope companies, including Lantheus Medical Imaging, ISOFLEX and SPEC; along with commercial uranium suppliers. Establishing these relationships and obtaining the required licenses has positioned Niowave to become a leading domestic producer of medical and industrial isotopes.

The key accomplishments from Phase II are summarized below:

- A 40 MeV superconducting electron linac has been designed and the development path for the hardware plotted
- A converter/target unit for photonuclear production of isotopes have been designed, built, and tested using a 40 MeV electron linac at the Idaho Accelerator Center. Radioisotope yields were simulated using Monte-Carlo techniques and experimentally measured. The results were found to be in good agreement.
- Radioisotope production via neutron capture has been investigated. A prototype of the neutron source was designed, built, and tested using a 40 MeV electron linac at the Idaho Accelerator Center. Radioisotope yields were simulated using Monte-Carlo techniques and experimentally measured. The results were found to be in good agreement.
- A dedicated radioisotope production facility was designed and was built in Lansing, MI with beneficial occupancy obtained in February 2015. The facility will include a gamma-spectroscopy laboratory, hot cells, and processing units.
- Niowave has received approval of the shielding plan for electron beams up to 40 MeV and 100 kW at the Airport Facility from the state's department of Licensing and Regulatory Affairs (LARA) radiation safety section. Niowave has two NRC license applications approved: 1) to possess, machine, and perform R&D work with natural and depleted uranium as well as natural thorium; and 2) for production of R&D quantities of radioisotopes from stable targets and uranium, including a license to possess low enriched uranium (LEU).
- Partnerships have been established with ISOFLEX and SPEC, two commercial isotope distributors. Both companies are interested in purchasing several medical and industrial radioisotopes.

LINAC DESIGN

In the first year of the project, a modular design for a 40 MeV linac was prepared based on existing technology. A 350-MHz normal-conducting electron gun driven by a thermionic cathode is followed by a 6 MeV superconducting double spoke at double the source frequency serving as booster and buncher. Following the buncher is three 12-MeV superconducting double spokes at the fundamental frequency with 12 MeV of energy gain each. In year two, the superconducting cavity designs have been replaced by a Niowave reentrant-cell design with sufficient RF acceptance that it can be used with the non-relativistic beam, eliminating the need for a separate booster/buncher design. This new design is a nominally 10 MeV cavity at CW, with conservative field levels so that double the gradient should be achievable with pulsing. The path toward the 100 kW machine at 40 MeV then involves the demonstration of the full system at low duty cycle with two cryomodules and then 100% duty with four. Since all the modules are substantially the same, costs are reduced both at the development stage and in full production.

The hardware development path has been initiated. The electromagnetic designs for a single 3.3 MeV energy gain reentrant cell and multiple cell cavities were elaborated using the Poisson Superfish [Halbach K and Holsinger R F,"SUPERFISH -- A Computer Program for Evaluation of RF Cavities with Cylindrical Symmetry," Part. Accel. 7 (1976) p. 213–22] and CST Microwave Studio [Computer Simulation Technology AG,"CST Computer Simulation Technology," http://www.cst.com] computer codes. An important trade-off investigated during the design was between the cell-to-cell coupling and peak magnetic fields. More coupling increases peak fields in the coupling cells, but simplifies the process of field flatness tuning. However, with only three cells, field flatness tuning is easily achieved –low cell-to-cell coupling and low peak magnetic fields in the coupling cell are preferred. Mechanical designs for one-, two-, and three-gap reentrant structures based on this Niowave cell shape have been completed and progress has been made on fabrication and cryotesting to demonstrate the cell shape and the cell-to-cell coupling.

Preliminary testing with beams from Niowave normal-conducting electron guns (thermonic cathode driven) are also underway. The common beamline design planned for many of these tests contains focusing and steering elements that allow the electron bunches at 50-100 keV to be properly matched into the superconducting cavity RF acceptance. A photograph of the normal-conducting electron gun in commissioning is shown in Figure 1 and a full accelerator (with a single-gap prototype SRF accelerating cavity) is shown in Figure 2.

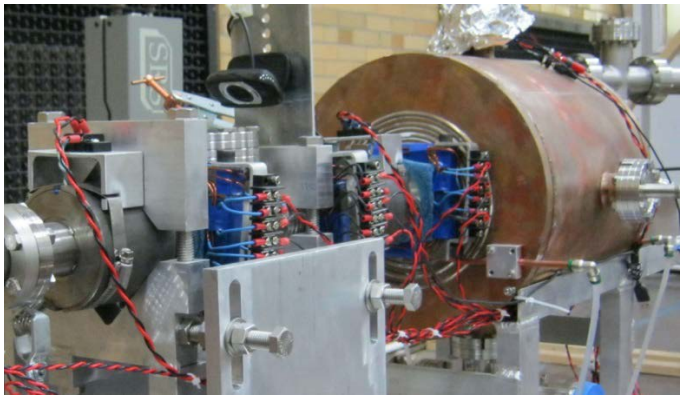

Figure 1. A Niowave normal-conducting electron gun in commissioning.

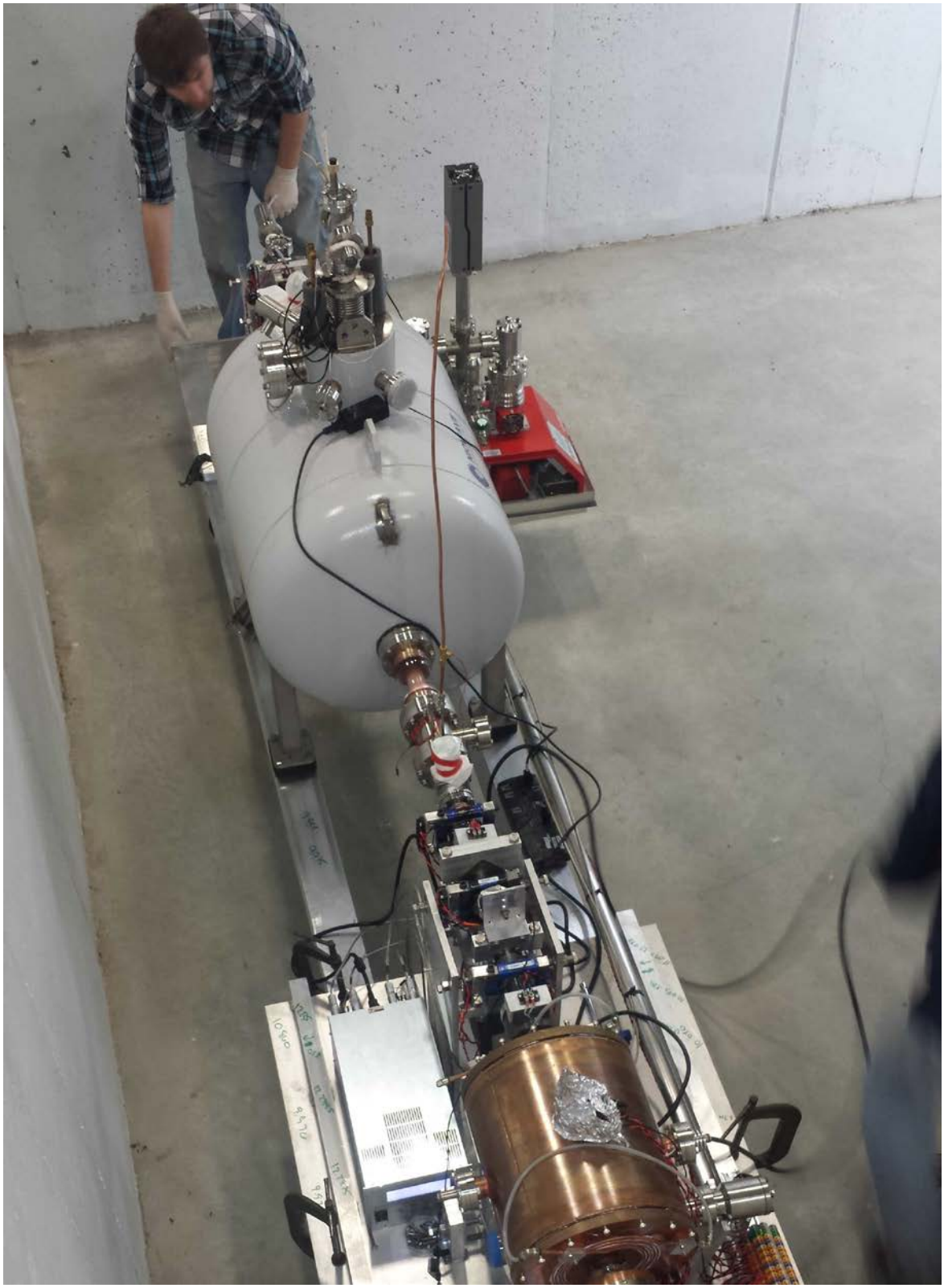

Figure 2. A single-cell cryomodule with normal-conducting electron gun and beamline being installed into the testing tunnels at Niowave for first beam testing.

Figure 3. The high-power test facility at the Niowave headquarters. The two tunnel layout with roof access for cryogenics served as the model for the isotope production facility at the Lansing, Michigan airport.

Development of high-power accelerators is continuing at the Niowave Electron R&D building, the high-power test facility at Niowave headquarters in Lansing, Michigan (see Figure 3). This building is licensed to operate up to 40 MeV and 100 kW of beam power. The electron beam diagnostics and high-power RF sources and couplers will be upgraded as the beam power is increased towards the full design. Demonstration of the feasibility of isotope production processes will occur here, and full isotope production runs will happen at a similarly-designed building at the Lansing airport, discussed below.

PHOTONUCLEAR PRODUCTION OF RADIOISOTOPES

Bremsstrahlung radiation

As the primary beam electrons are slowed down by the electric field surrounding the nuclei of the atoms in the converter, the Coulomb field of an atomic nucleus causes electron acceleration and bremsstrahlung radiation. The effect is two-fold: one is electron-nucleus radiation (ENR) and the other one is electron-electron radiation (EER). ENR is the dominant form of bremsstrahlung radiation due to the pronounced dipole moment radiation and the high probability of interaction with greater charge of the nucleus or atom. The primary-beam electrons lose energy and change direction due to inelastic scattering in the sample. Some of the lost energy is converted to x-rays which have a range of energies, from zero up to the energy of the electrons in the primary beam. Bremsstrahlung x-ray spectrum have a characteristic shape approximately described by Kramer's' law. Figure 4 shows a cartoon of the bremsstrahlung radiation process (left) and distribution of photon energies simulated for 10 MeV and 40 MeV

electron beam hitting a 4 mm thick tungsten converter (right). The resulting high-energy photons can cause numerous photonuclear reactions.

Photoneutron (γ,n) and photoproton (γ,p) production

Photonuclear reactions can be described as a two-stage process. During the first stage a photon is absorbed, and a nucleus becomes excited. During the second stage, the excitation energy is released – in the form of a photon, neutron, or a charged particle (proton, alpha particle, etc). Photonuclear reactions, integrated over a broad bremsstrahlung spectrum, can transmute a significant fraction of the target material, as demonstrated by numerous reports on photonuclear production of isotopes [3, 4, 5]. Multi-kilowatt electron accelerators, with beam energies of about 40 MeV, produce extremely high Giant Dipole Resonance (GDR) photon flux. The term "GDR-photons" is used to refer to the photons with energies between 10 and 40 MeV, where the photonuclear cross-section is at its peak. The GDR-photons excite the target nuclei causing particle emission and hence transmutation reactions. A proper converter can provide more than 10^{16} photons/cm^2/s per kW of electron beam power.

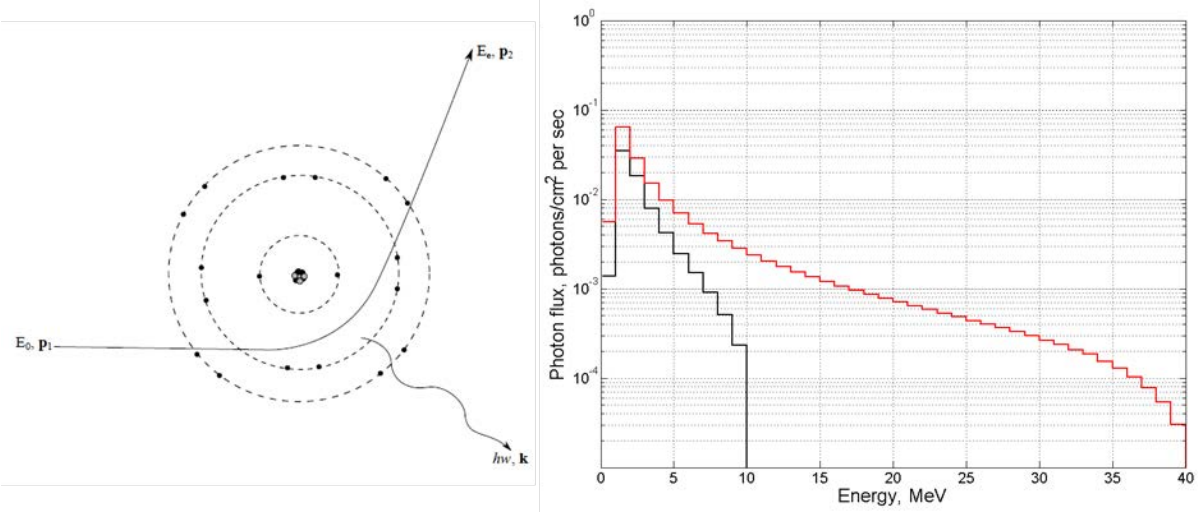

Figure 4. Left: Bremsstrahlung radiation process. Right: Bremsstrahlung spectra simulated for 10 MeV and 40 MeV electron beam hitting a 4 mm thick tungsten converter.

Photoneutron (γ,n) and photoproton (γ,p) production

Photonuclear reactions can be described as a two-stage process. During the first stage a photon is absorbed, and a nucleus becomes excited. During the second stage, the excitation energy is released – in the form of a photon, neutron, or a charged particle (proton, alpha particle, etc). Photonuclear reactions, integrated over a broad bremsstrahlung spectrum, can transmute a significant fraction of the target material, as demonstrated by numerous reports on photonuclear production of isotopes [6, 7, 8]. Multi-kilowatt electron accelerators, with beam energies of about 40 MeV, produce extremely high Giant Dipole Resonance (GDR) photon flux. The term "GDR-photons" is used to refer to the photons with energies between 10 and 40 MeV, where the photonuclear cross-section is at its peak. The GDR-photons excite the target nuclei causing

particle emission and hence transmutation reactions. A proper converter can provide more than 10^{16} photons/cm^2/s per kW of electron beam power.

The production rate of the isotope depends on a number of parameters, such as the the threshold energy of the nuclear reaction $\boldsymbol{E_{th}}$, the maximum energy of photons $\boldsymbol{E_{max}}$, the photon flux density $\boldsymbol{\varphi_\gamma(E)}$, and the cross-section of a photonuclear reaction $\boldsymbol{\sigma_{(\gamma,x)}(E)}$:

$$\frac{dN}{dt} = \int_{E_{th}}^{E_{\max}} \varphi_\gamma(E) \cdot \sigma_{(\gamma,x)}(E)\, dE_\gamma . \tag{1}$$

If the target is significantly large so that the photon flux is not uniform throughout the target, the production rate should be calculated as:

$$\frac{dN}{dt} = \int_{E_{th}}^{E_{\max}} \int_V N(\vec{r})\varphi(E,\vec{r}) \cdot \sigma(E)\, dE d^3\vec{r}, \tag{2}$$

The yield of the radioisotope produced in the sample after irradiation time of $\boldsymbol{t_{irr}}$ can be found from the production rate as:

$$Y(t) = N_T \frac{dN}{dt}(1 - e^{-\lambda t_{irr}}), \tag{3}$$

where $\boldsymbol{N_T}$ is the number of target atoms in the sample and $\boldsymbol{\lambda}$ is the decay constant of the produced isotope.
Below are some examples of important medical radioisotopes which can be produced via photoneutron and photoproton reactions:

$$^{100}Mo + \gamma \rightarrow ^{99}Mo + n, \tag{4}$$

and

$$^{48}Ti + \gamma \rightarrow ^{47}Sc + p. \tag{5}$$

Generally speaking, to maximize the yield of the isotopes produced by the photoneutron or photoproton method, the electron beam current needs to be maximized. Increasing the beam energy also results in a higher yield of the desired isotope. However, higher energy can also open higher order channels, such as (γ, 2n) and (γ, np), which often produce unwanted byproducts and complicate the separation process. Careful analysis is necessary to find the optimum irradiation parameters for each target material. Also, converter design will affect the flux. An optimum thickness exists for each material and electron energy.

Neutron capture (n,γ)

Due to their lack of charge, slow neutrons do not have to hurdle the Coulomb potential of atomic electrons and can relatively easy find themselves in the vicinity of the nucleus. Once in close proximity to the nuclei, they are easily captured and the nucleus becomes excited.

An example of such reaction is:

$$^{196}Au + n \rightarrow ^{197}Au + \gamma. \quad (7)$$

The neutron capture cross-section decreases as energy increases as seen in Figure 8 showing the neutron capture cross-section for ^{196}Au(n,γ)^{197}Au reaction. Adding a carefully designed moderator and reflector around the converter is absolutely necessary to thermalize the neutrons and obtain high isotope yield.

The production rate of the isotope produced via neutron-induced excitation can be calculated similarly to Eq. 1:

$$\frac{dN}{dt} = \int_{E_{th}}^{E_{max}} \varphi_n(E) \cdot \sigma_{(n,\gamma)}(E)\, dE_n, \quad (8)$$

where $\boldsymbol{\varphi_n(E)}$ is the neutron flux density, and $\boldsymbol{\sigma_{(n,\gamma)}(E)}$is the cross-section of a neutron capture reaction. The yield of the radioisotope produced in the sample after irradiation time of $\boldsymbol{t_{irr}}$ can be found can be found according to Eq.2. An optimized converter design can provide more than 10^{14} neutrons/cm^2/s per kW of electron beam power.

In reality, placing a high Z material in the electron beam with energies above the (γ,n) reaction always creates both photon and neutron fields and opens up all three channels: (γ,n/p), (n,n'), and (n,γ). By modifying the design of the converter, moderator, and reflector; it is possible to optimize the system for either high photon flux (which maximizes photoabsorption), fast neutron flux (which maximized inelastic neutron scattering), or thermal neutron flux (which maximizes neutron capture).

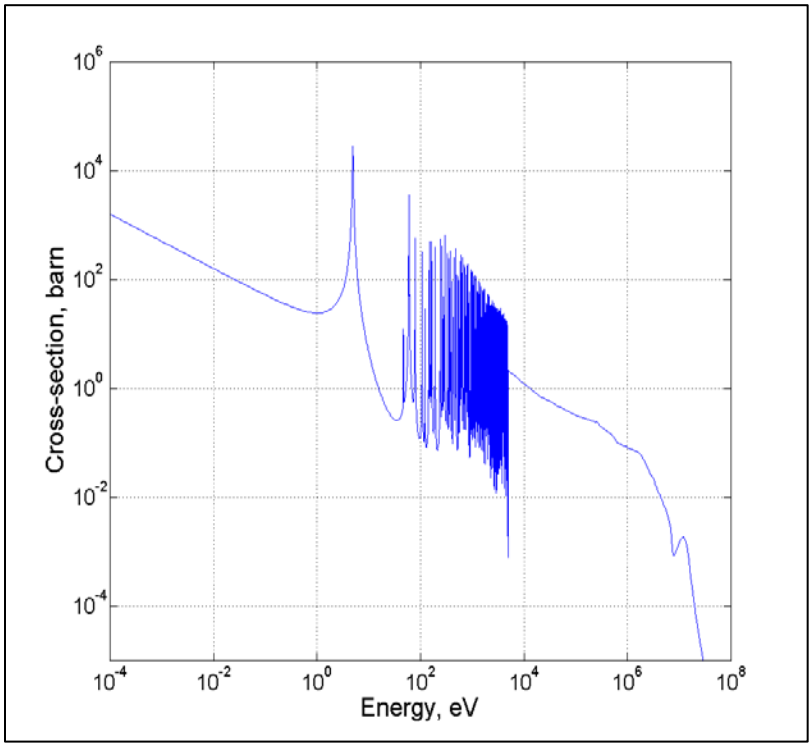

Figure 5. Neutron capture cross-section for ^{196}Au.

TARGET/CONVERTER DEVELOPMENT

One of the first tasks we have accomplished was finding the optimum converter thickness and material to maximize the photon/neutron flux and the isotope production rate. Typical bremsstrahlung converter materials have high atomic number and density, and include tungsten, tantalum, platinum, lead, and gold. Their properties are summarized in Table 1.

Table 1. Physical properties of some commonly used converter materials.

Element	Atomic number (Z)	Density, g/cm^3	Melting point, °C
Tantalum (Ta)	73	16.7	3,017
Tungsten (W)	74	19.3	3,422
Platinum (Pt)	78	21.5	3,215
Gold (Au)	79	19.3	1,064
Lead (Pb)	82	11.3	327
Bismuth (Bi)	83	9.8	271

Lead-bismuth eutectic (LBE) containing 45% of lead and 55% of bismuth was chosen as the liquid metal converter material. Both lead and bismuth have high atomic numbers and good conversion efficiency. In addition, the eutectic quickly solidifies in case of a leak and therefore cannot create an explosion. Activation products of LBE are listed in Table 2. To maintain LBE circulation we proposed a vertical stainless steel loop filled with LBE and kept one arm of the loop at a higher temperature than the other arm (see Figure 6). The density of the LBE decreases as the temperature increases (see Figure 7) as [9]:

$$\rho(T)[kg/m^3] = 11{,}096 - 1.3236 \cdot T(K) \tag{9}$$

Table 2. Possible photon activation products of LBE.

Reaction	*Half-life*	*Emitted gammas (and corresponding branching ratios)*
Pb-204(γ,n)Pb-203	52.1 h	280 keV (80%)
Pb-204(γ,2n)Pb-202m	6.6 h	422 keV (86%), 961 keV (92%)
Pb-204(γ,3n)Pb-201	9.4 h	331 keV (78%)
Pb-206(γ,2n)Pb-204m	67 min	374 keV (90%), 899 keV (99%), 912 keV (96%)
Bi-209(γ,2n)Bi-207	38 d	570 keV (98%), 1064 keV (74%)
Bi-209(γ,3n)Bi-206	6.2 d	516 keV (41%), 803 keV (99%), 881 keV (67%)

Having the temperature gradient of about 100 degrees K between the arms will result in about a 200 kg/m^3 difference in the LBE densities (assuming the temperature remains relatively constant throughout the arm). Thereby the LBE in the "cold" arm will sink, and LBE in the "hot" arm will rise, thus establishing natural circulation in the loop.

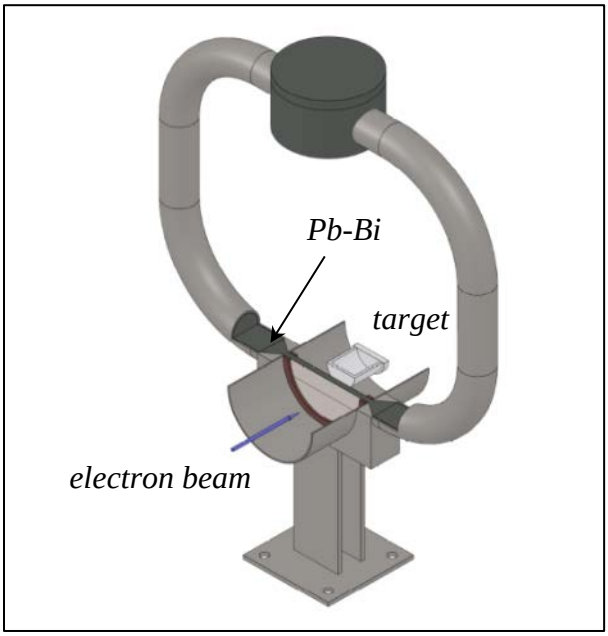

Figure 6. Conceptual design of the high-power LBE converter.

Wrapping several heat tapes around the loop is necessary to melt the LBE (starting from the top) and get it moving. Experiments at Niowave demonstrated that temperature gradient as low as 40 degrees K provided a sufficient pressure head to overcome friction in the loop and sustain slow LBE circulation. Increasing ΔT results in higher LBE flow rate. Once the circulation is established, the electron linac can be turned on, so that the beam will hit the converter region - a flat 2 mm thick layer of LBE sandwiched between two 0.25 mm thick stainless steel windows. The power deposited into the LBE (and stainless steel windows) will keep the eutectic melted and circulating, and the heat will be carried away by the rising LBE.

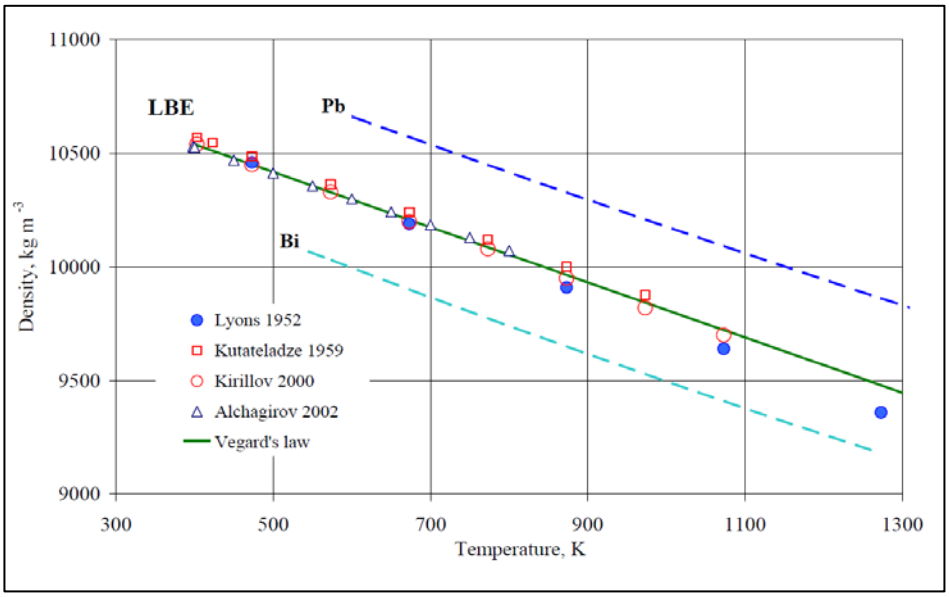

Figure 7. Density of the melted LBE versus temperature. Adopted from [3].

The loop was also tested at the Idaho Accelerator Center (see Figure 8 and Figure 9 for the conceptual setup and actual photo). Six thermocouples were inserted to control the temperature of the eutectic during the irradiation. To evaluate conversion efficiency of the Pb-Bi eutectic, a

sample of natural Zn was placed behind the converter. Seven readouts were done simultaneously – six of them were coming from different regions of the loop and one from the Zn sample (see Figure 10). The loop was warmed up to the operating temperatures of about 250-280 degrees C (depending on the position of the thermocouple in the loop) and placed in the electron beam from the 48-MeV linac housed in the main IAC building.

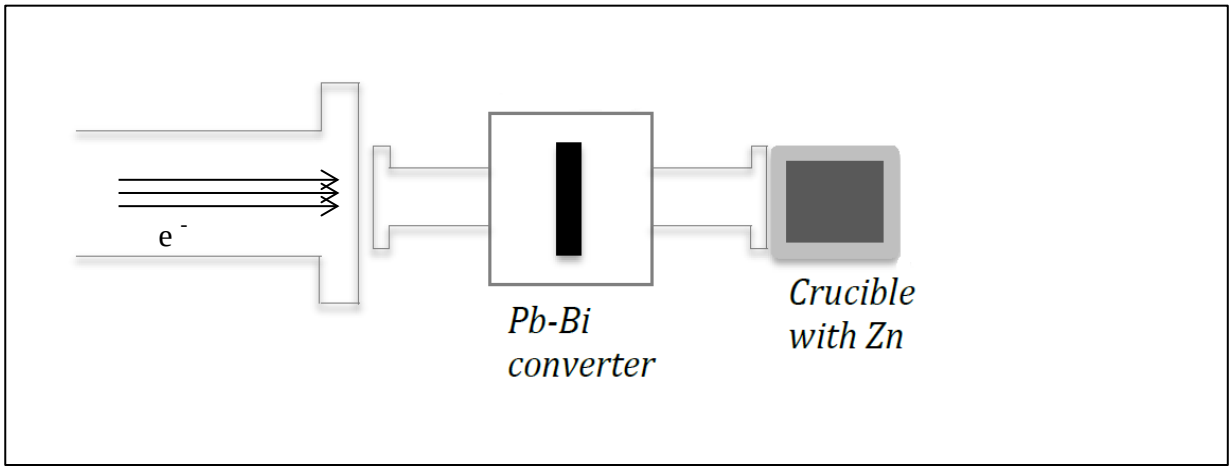

Figure 8. Conceptual layout of the experimental setup for the July 2013 experiment at the IAC.

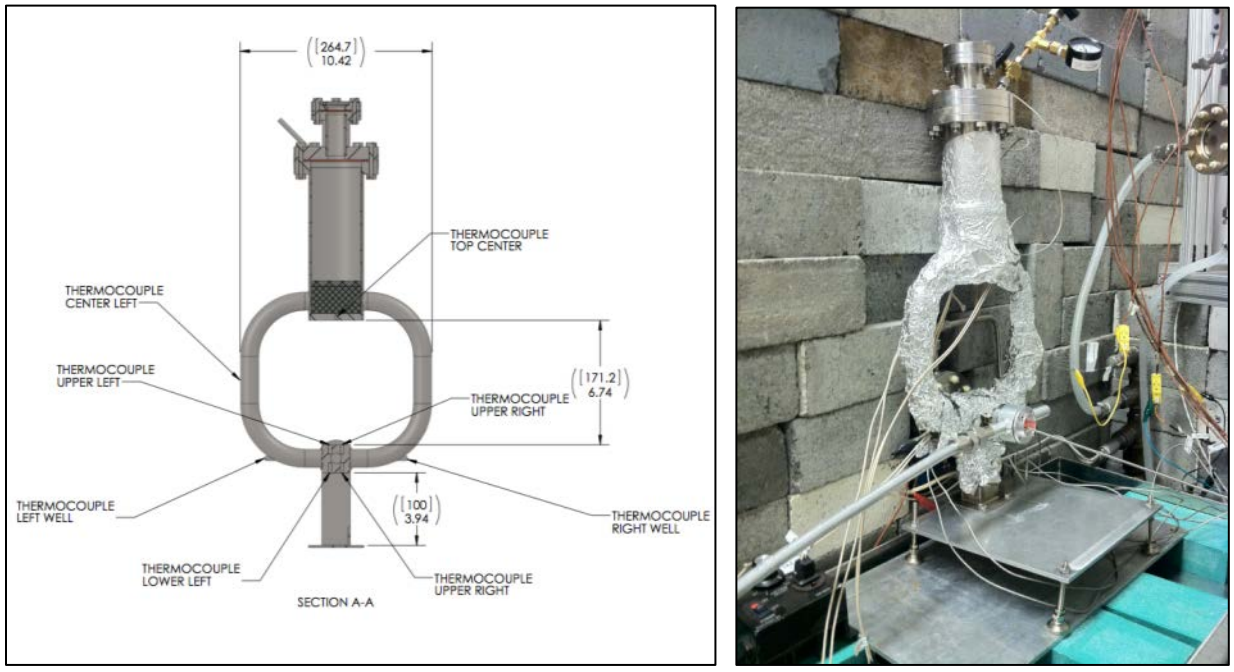

Figure 9. Pb/Bi loop. Left: Conceptual design. Right: Loop in front of the electron beam line, July 2013.

The linac we used for this experiment is composed of two 2856 MHz sections. The first is a standard standing wave, side coupled cavity, buncher/pre-accelerator injecting a 27 MeV beam (unloaded) into the second section, which is a standard SLAC type traveling wave accelerator. Each section is provided with microwave power from its own klystron (5 MW peak output). The

total unloaded output energy is ~ 48 MeV, and the optimum electron beam energy providing the highest average beam current is about 42 MeV. The irradiation was performed in four 10 minute intervals with the electron beam power increasing from ~ 300 W to ~ 1 kW a total integrated incident energy of 0.4 kW·h. The results of the temperature readings from the thermocouples are shown in. The Zn target temperature did not exceed 150 degrees C even at 1 kW.

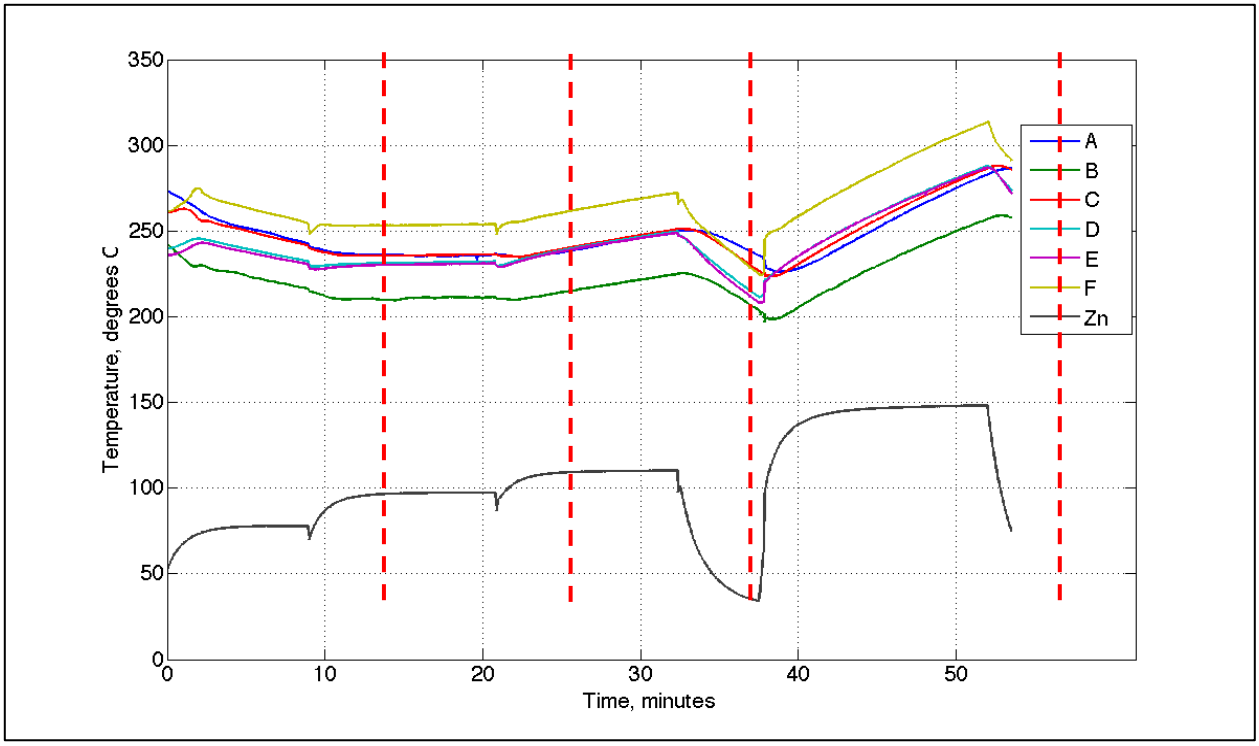

Figure 10. The results of the temperature readings from the thermocouples.

Isotopes produced with photonuclear reactions

During Phase II of the project we focused on several isotopes which can be produced via photonuclear method. Some of them were medical (Cu-67, Ac-225), while others were industrial (Mn-54, Zn-65). The reactions of interest are listed below:

$$^{68}Zn + \gamma \rightarrow ^{67}Cu + p,$$
$$^{226}Ra + \gamma \rightarrow ^{225}Ra + n \rightarrow ^{225}Ac,$$
$$^{55}Mn + \gamma \rightarrow ^{54}Mn + n,$$
$$^{66}Zn + \gamma \rightarrow ^{65}Zn + n.$$

Their properties are summarized in Table 3 and their photonuclear cross-sections are shown in Figure 11.

Table 3. Properties of some of the isotopes of interest.

Product	Target abundance, %	Reaction	Half-life	Threshold energy, MeV	Integral cross-section (from 0 to 40 MeV), MeV*mb
Cu-67	18.8	(γ, p)	67 hours	10	164
Ac-225	100	(γ, n)	10 days	7	1148
Mn-54	100	(γ, n)	107 days	10	445
Zn-65	28	(γ, n)	244 days	11	634

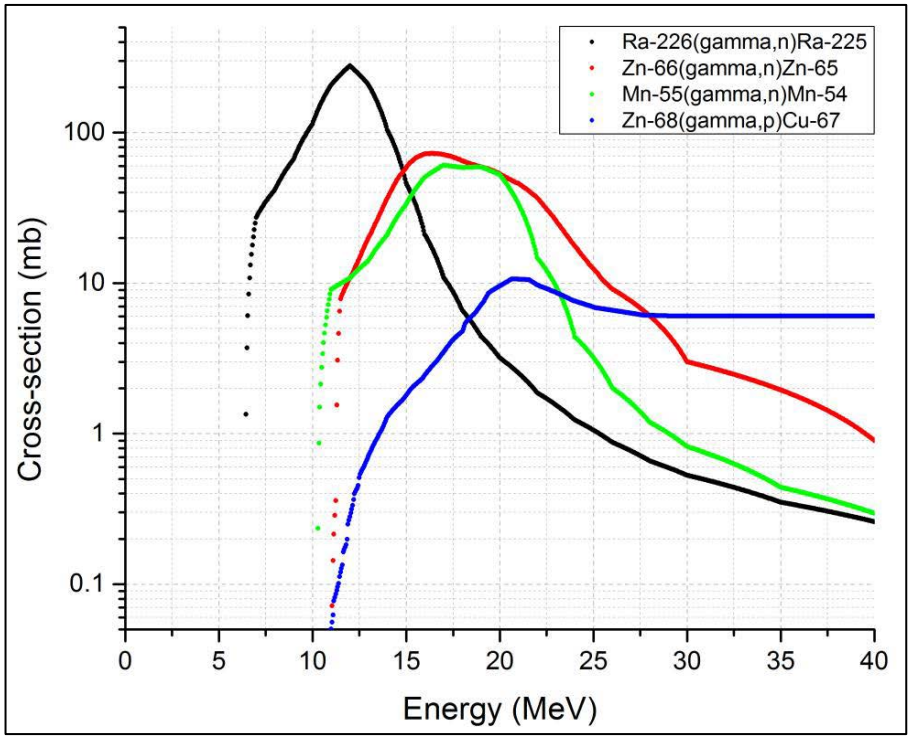

Figure 11. Cross-sections adopted from:Ra-226(γ,n)Ra-225 – TENDL, Zn-66(γ,n)Zn-65 – Goryachev (1968) and KAERI, Mn-55(γ,n)Mn-54 – TENDL, Zn-68(γ,p)Cu-67 – KAERI.

MCNPX simulations of the yields

To accurately predict the production rate we used MCNPX, a general purpose particle transport Monte Carlo code, developed by the Los Alamos National Laboratory (Pelowitz, 2008). MCNPX involves source characterization, target material and geometry specifications, physics process management, and output - tallies of the physical quantities of interest. For example, bremsstrahlung fluxes can be simulated using F4 tallies (photon flux averaged over a cell). The results of such simulations of the photon flux through the Zn target are shown in Figure 12. Similar simulations were done for all the isotopes of interest.

To estimate the yield, the integral (1) was evaluated by simulating bremsstrahlung fluxes multiplying them with ENDF/B-VII cross-sections (Chadwick et al, 2006) utilizing FM tally multiplier card. The FM card is used in MCNPX to calculate any quantity of the form:

$$FM = C\int \varphi(E)\cdot R(E)\,dE, \qquad (6)$$

where φ(E) is the energy-dependent fluence (particle/cm^2), R(E) is an energy-dependent function, and C is a constant. In particular, if the cross-section σ(E) of certain reaction is chosen to be the energy-dependent function R, and constant C is properly defined, the FM card allows calculating the production rate of the radioisotope. For example, irradiating a cylindrical sample (0.8 cm in diameter, 2.6 cm long) of natural zinc, the activity of Cu-67 was predicted to be about 20 μCi/(g*kW*h) and the activity of Zn-65 was predicted to be about 2.5 μCi/(g*kW*h). Similar calculations were done for Ac-225 and Mn-54 yields.

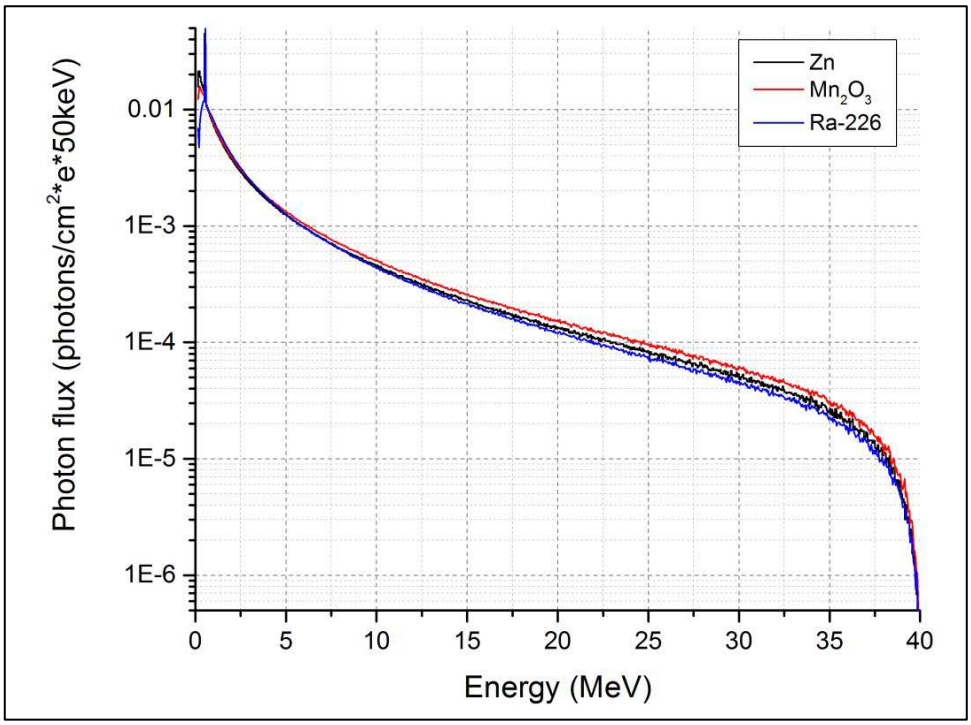

Figure 12. Average photon flux through the Zn, Mn_2O_3 and ^{226}Ra targets (targets are cylindrical, 0.8 cm in diameter, 2.6 cm long)

Measurements of the yields at the Idaho Accelerator Center

On May 15th, 2013 we have activated an alumna crucible filled with 40 g of natural zinc (see Figure 13). The irradiation lasted 1 hour and the electron beam energy was 40 MeV. The beam power changed during the experiment: it was 202 W for the first 10 minutes of irradiation, 531 W for the second 10 minutes of irradiation, and 700 W for the remaining 40 minutes. Total Power*Time was 0.59 kW*hr. The sample was removed from the experimental cell on Thursday, May 16th at 8:30 am and its activity was measured using high purity germanium detector. Gamma-spectra are shown in Figure 14. The experimental results were compared with the predicted values (see Table 4), and were found to be in good agreement.

Figure 13. Zn irradiation setup. Thermocouple is inserted for temperature measurements. Cold air is blowing on both converter and target.

Table 4. Predicted and measured activities of Cu-67 and Zn-65.

Measured activity, μCi/(g kW·hour)		
	Cu-67	Zn-65
1	15.5	2.1
2	16.4	2.2
3	15.8	2.1
4	16.2	2.2
Average:	16.0±0.4	2.15±0.05
Predicted activity, μCi/(g kW·hour)		
	20	2.5

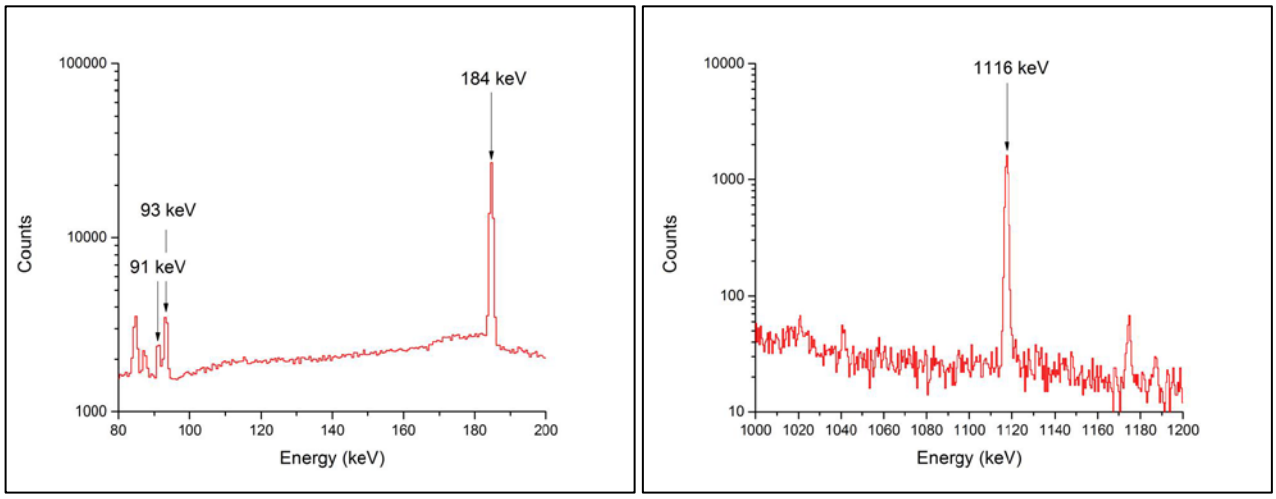

Figure 14. Gamma-spectra showing Cu-67 line (left) and Zn-65 line (right).

Isotopes produced via neutron capture

During Phase II of the project we focused on several isotopes which can be produced via the photonuclear method. To monitor neutron flux we investigated the following reactions:

$$^{197}Au + n \rightarrow ^{198}Au + \gamma,$$

$$^{55}Mn + n \rightarrow ^{56}Mn + \gamma.$$

In order to find out neutron and photon flux distribution, MCNPX simulations were done for different electron beam energies. Optimum converter thicknesses were determined based on maximum neutron flux generation. An example of such neutron flux simulation is shown in Figure 15.

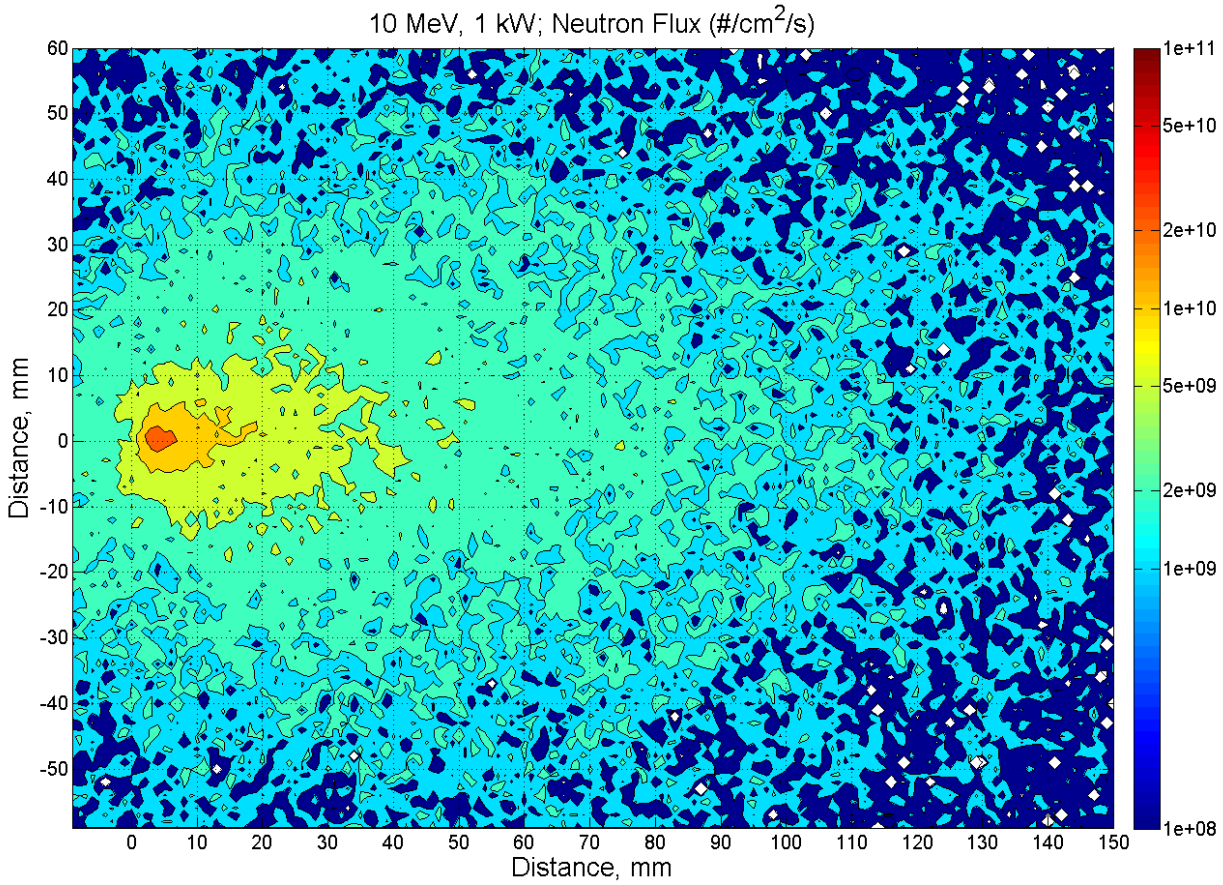

Figure 15. MCNPX simulations of neutron flux for 10 MeV electron beam incident on LBE.

Optimum converter thicknesses were simulated for different energies (seeTable 5). Thick LBE converter was designed, built, and used for neutron capture in gold and manganese. MCNPX simulations were done to predict the yields of the produced isotopes. The samples were submerged into a large (1ft x 1ft x 1ft) tank of H_2O or D_2O. A schematic of the experimental set up is shown in (see Figure 16) where the locations of the activations foils are indicated by #1-#4.

Table 5. Beam energies and associated converter thicknesses

Beam Energy	Converter Thickness
10 MeV	3 mm
20 MeV	6 mm
40 MeV	10 mm

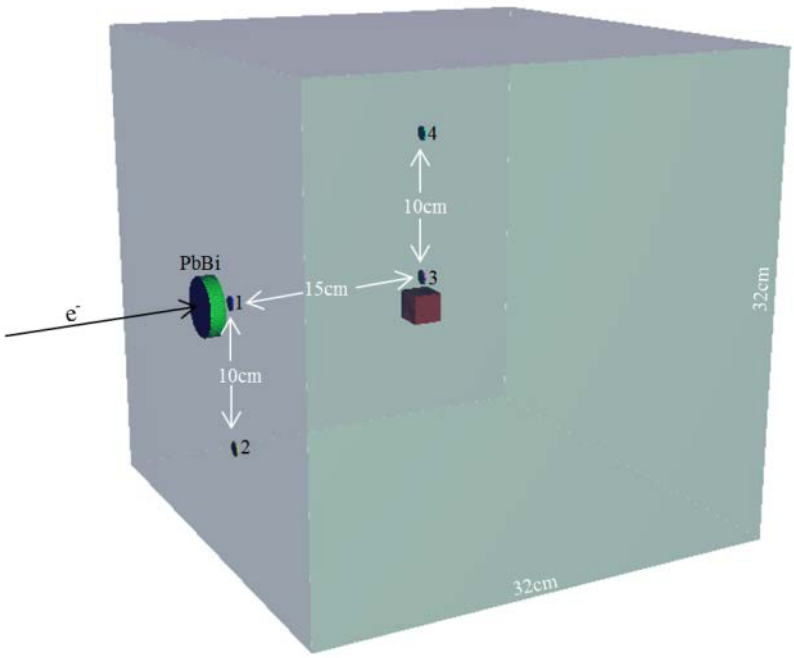

Figure 16. A schematic of the experimental setup showing the positions of the Mn and Au activation foils inside an H_2O or D_2O tank.

Measurements of the yields at the Idaho Accelerator Center

To measure the predicted yields of the isotopes produced via neutron capture we used an electron linac (the Short Pulse Linac at the Idaho Accelerator Center) operating at three different energies of 10, 20 and 40 MeV. The electrons from the accelerator impinged upon solid lead bismuth ingots generating bremsstrahlung photons. The PbBi bremsstrahlung converter was immersed in a tank of deuterated water (D_2O) of dimensions 1' x 1' x 1' (see Figure 17). The purpose of the deuterated water was twofold. First, neutrons were generated via the $^2H(\gamma,n)$ reaction. Second, the D_2O served as the moderator for the neutrons. For benchmarking purposes, runs were performed with identical setups except the D_2O was replaced with deionized H_2O. Photon and thermal neutron fluxes were measured for each incident electron beam energy via a set of eight activation foils placed at four locations throughout the D_2O/H_2O moderator.

The accelerator used in these measurements was a 1300 MHz (L – band) RF linac capable of energies ranging from 2 to 44 MeV. Its pulse width is variable from about 60 picoseconds to 2 microseconds, and its repetition rate can be varied from single pulse to 180 Hz. The charge per pulse is also adjustable. It has both zero degree and ninety degree ports. The latter has variable energy slits for momentum definition. In these measurements, the ninety degree port was utilized, and the energy (10, 20, and 40 MeV), pulse width, charge per pulse and repetion rate were varied to obtain the desired power. Data were taken with the energy defining slits open, resulting in an estimated electron beam energy spread of +- 1 MeV.

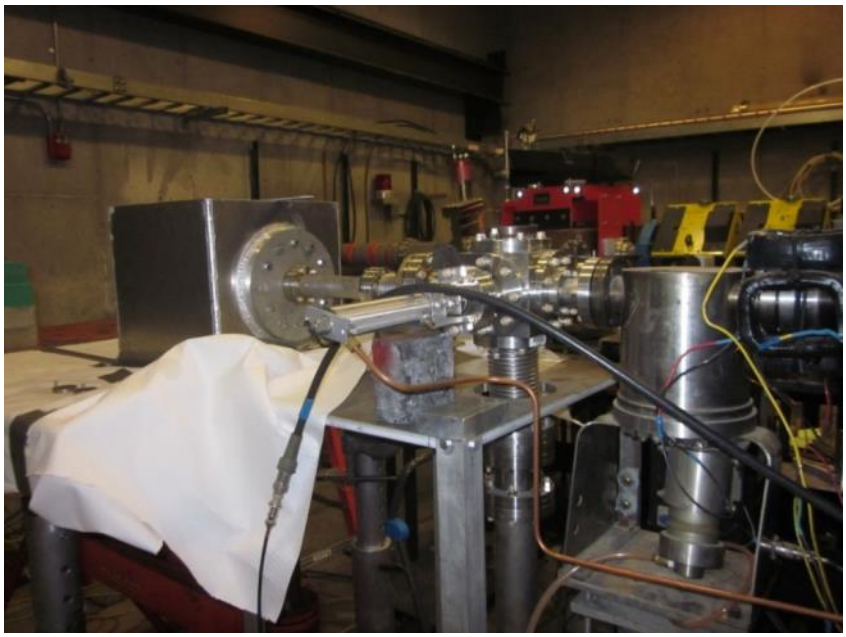

Figure 17. A photograph of the experimental setup. The electron beam enters from the right and, upon exiting a stainless steel vacuum window, impinges upon a PbBi converter which is immersed in the D_2O/H_2O on the upstream side.

The LBE converters consisted of 1.5” diameter disks of PbBi (56% Bi, 44% Pb, melting point 255 degrees F, product number 8921K14 obtained from McMaster-Carr). They were fabricated by melting the material in the mold shown in Figure 18(left). After melting in the mold, the LBE converters were cooled to room temperature and then placed in liquid nitrogen to extract them from the mold.

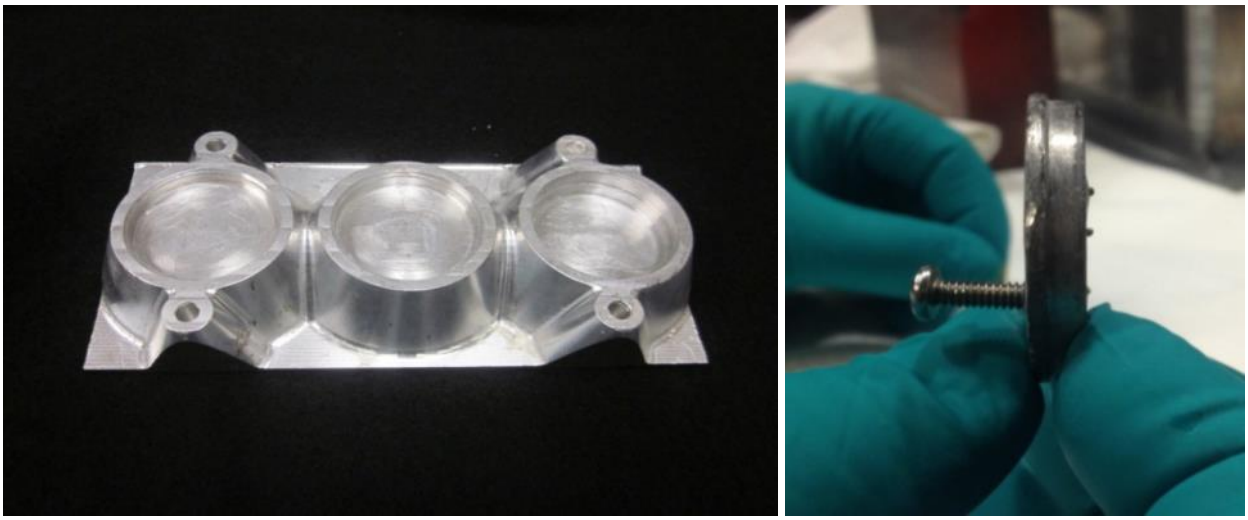

Figure 18. Left: Mold used in the fabrication of LBE converters.
Right: Side view of one of the converters.

As indicated in Figure 19, these converters were placed on the upstream side of the D_2O/H_2O tank. They were flush with the vacuum window which comprised the exit port of the electron accelerator.

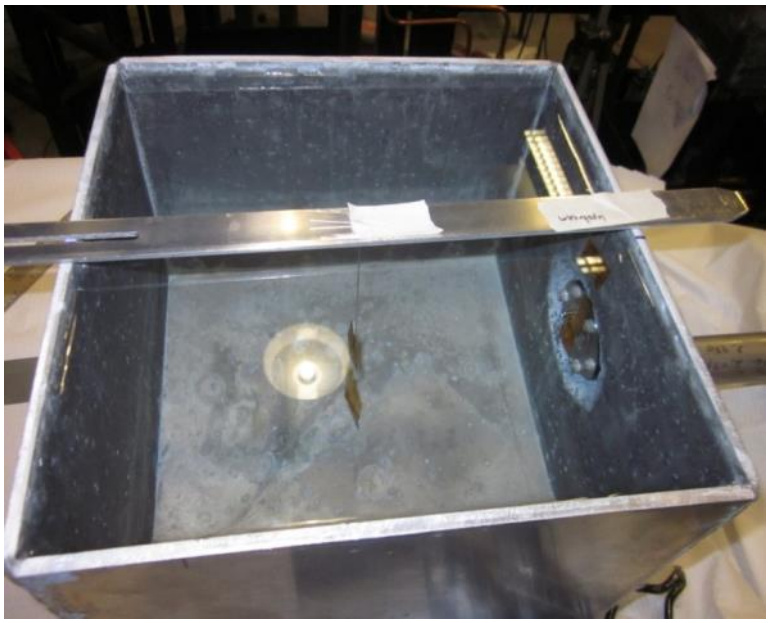

Figure 19. A photograph from the top of the apparatus showing a set of Au and Mn activation foils and the LBE converter (right).

In the course of the measurements, some melting of the PbBi was observed at 20 MeV using H_2O and at 10 MeV for both moderators (see Figure 20). Each converter was remade if it was damaged to ensure each run started with a smooth, undamaged converter.

Figure 20. Melting damage done to the LBE converter – 10 MeV, D_2O moderator

While we were mostly interested in neutron capture reactions, we also estimated photonuclear production of isotopes, in particular ^{54}Mn and ^{196}Au. We used manganese and gold foils in order to see both a (n,γ) reaction and a (γ,n) reaction from each metal. For the Mn samples, we used pieces of a shattered Mn plate. We attached two roughly similar pieces together with kapton tape in order to make a small packet. These packets were 2.13 ± 0.05 g each. The Mn pieces have an area of 1.0 ± 0.4 cm² and were trimmed and assembled so that the packets were more or less square in shape. The gold foil masses were 0.125 ± 0.001 g and were circular with a diameter of ½ inch. For 10 MeV, we had a very low projected activity per gram. So for the 10 MeV runs, we used three gold foils stacked together, with each packet of three having a mass of 0.377 ± 0.003 g. Each packet of Mn and Au taped together had a designation of its beam energy, its moderator, and its tank position. For example, 10-1H would mean the activation packet used in the 10 MeV run, at position 1, using H_2O as the moderator. In this way, the packets were labeled and we were able to keep track of them. The foils were placed in the tank with the Au side facing downstream, and the Mn on the upstream side. Activation packet #1 was directly behind the converter, and # 3 was 15 cm behind the converter. Packets # 2 and #4 were

off axis as indicated in Figure 16. Table 6 shows the isotopes of interest for Au and Mn for this experiment.

Table 6. Isotopes of interest.

Target Material	Reaction	Isotope of Interest	Half Life	E_γ (keV)
Mn	^{55}Mn (n,γ) ^{56}Mn	^{56}Mn	2.58 hours	847,1811,2113
Mn	^{55}Mn (γ,n) ^{54}Mn	^{54}Mn	312.3 d	835
Au	^{197}Au (n,γ) ^{198}Au	^{198}Au	2.7 days	412
Au	^{197}Au (γ,n) ^{196}Au	^{196}Au	6.18 d	356

The natural abundance of ^{55}Mn is 100%. The intensities for the 847, 1811, and 2113 keV lines in ^{56}Mn are 98.9%, 26.9%, and 14.2% respectively. The intensity for the ^{54}Mn line at 835 keV is 99.98%. The natural abundance of ^{197}Au is also 100%. The intensity for line in ^{198}Au at 412 keV is 95.6%, and the intensity for the 356 keV line in ^{196}Au is 87%.

The charge and current were monitored by means of a retractable water stop just upstream of the exit port of the accelerator. This apparatus is the vertical cylindrical can at the right of the picture. When inserted, it stops the electron beam and the charge per pulse is read off. While the presence of the D_2O and H_2O moderators did not in general allow a Faraday cup at the exit port, at one point when the tank was empty, a cross check with a Faraday cup was performed with excellent agreement. In addition, both the run time and the total number of electron beam pulses were recorded.

Activations were performed from November 18, 2014 to November 23, 2014. Each sample was counted the day of irradiation for at least 30 minutes. This allowed us to get the activity from ^{56}Mn before it decayed away. Most of the activation packets were recounted later for a long time in order to see the longer lived isotopes. Both the Au and the Mn activation samples were counted together for a given sample position and irradiation. Typical activation spectrum is shown below (Figure 21).

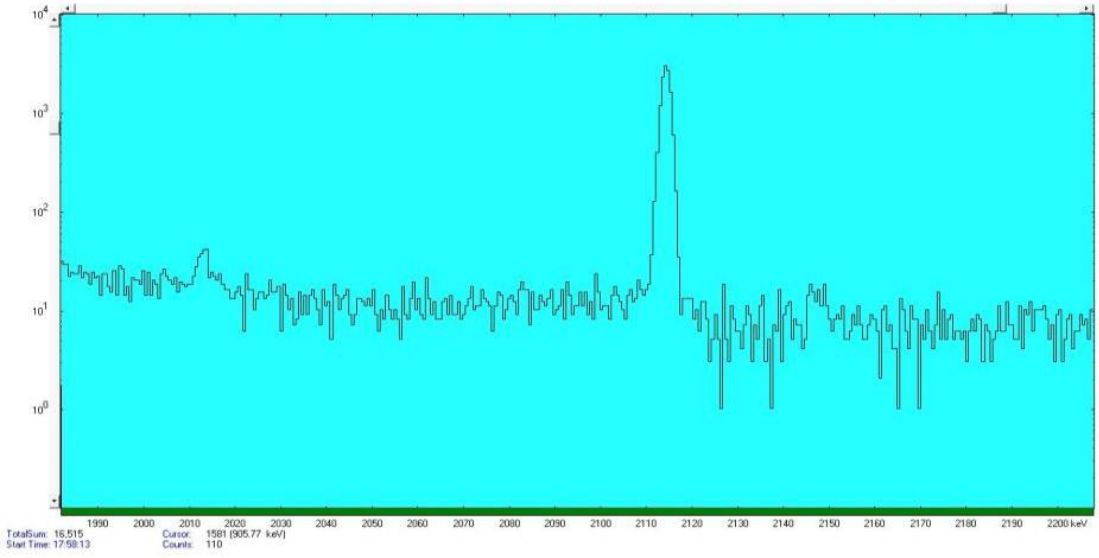

Figure 21. Example spectrum showing the 2113 keV line from 56Mn following the ^{55}Mn(n,γ)^{56}Mn reaction. The beam energy was 40 MeV and the moderator was D_2O.

The experiment was done on the L-band linac, on the 90 degree port. We used three energies; 40 MeV, 20 MeV, and 10 MeV. Table 7 shows the beam parameters used.

Table 7. Beam parameters

Beam Energy	H2O or D2O	Duration (min)	Beam Current (uA)
40	H	110	0.126
40	D	153	2.52
20	H	126	9.70
20	D	120	5.30
10	H	300	9.03
10	D	410	7.93

The following yield tables are organized as follows: each isotope and moderator combination has its own table. This table shows the activity (in μCi) per gram per micro amp for each beam energy at each tank position. All rates are decay corrected to correspond to the activity at the end of the irradiation. The following eight tables below are the results.

H_2O Moderator:

Table 8. μCi/g/μA for Mn-56 with H2O moderator.

Mn-56	Position 1	Position 2	Position 3	Position 4
40 MeV	118.5755	24.177419	27.950162	12.469477
20 MeV	2.5650242	1.5111242	2.7233774	1.3376991
10 MeV	0.2785787	0.0330322	0.01422	0.0042177

Table 9. μCi/g/μA for Mn-54 with H2O moderator

Mn-54	Position 1	Position 2	Position 3	Position 4
40 MeV	0.7016695	0.0019437	0.0660516	0.0159917
20 MeV	0.0443378	1.071E-05	0.0044868	0.0001387
10 MeV	1.03E-05	0	1.719E-06	0

.

Table 10. μCi/g/μA for Au-198 with H2O moderator.

Au-198	Position 1	Position 2	Position 3	Position 4
40 MeV	11.329682	1.843822	1.5280817	0.8373879
20 MeV	2.3953476	0.2374652	0.2961068	0.1514068
10 MeV	0.062109	0.0050436	0.00181	0.0005639

Table 11. μCi/g/μA for Au-196 with H2O moderator.

Au-196	Position 1	Position 2	Position 3	Position 4
40 MeV	25.878718	0.4426398	4.1546893	0.4345992
20 MeV	8.8932456	0.0045597	0.8580185	0.0397084
10 MeV	0.1907161	0.0001153	0.0104896	0.0004395

D_2O Moderator:

Table 12. μCi/g/μA for Mn-56 with D2O moderator.

Mn-56	Position 1	Position 2	Position 3	Position 4
40 MeV	19.201288	5.9367845	36.720038	26.053552
20 MeV	5.8934654	2.9135877	12.143374	8.8383785
10 MeV	3.1835496	1.3635082	6.6727901	4.411081

Table 13. μCi/g/μA for Mn-54 with D2O moderator.

Mn-54	Position 1	Position 2	Position 3	Position 4
40 MeV	0.4302312	0.0001556	0.0426975	0.0008408
20 MeV	0.0580549	4.426E-05	0.0051995	0.0002302
10 MeV	7.253E-06	0	0	9.534E-06

Table 14. μCi/g/μA for Au-198 with D2O moderator.

Au-198	Position 1	Position 2	Position 3	Position 4
40 MeV	4.77127	1.5715903	6.8722858	4.7680726
20 MeV	1.3883213	0.7047488	2.386641	1.6782802
10 MeV	0.962227	0.339794	1.5116656	0.9876479

Table 15. μCi/g/μA for Au-196 with D2O moderator.

Au-196	Position 1	Position 2	Position 3	Position 4
40 MeV	51.76362	0.0329944	4.8815225	0.1903545
20 MeV	11.182497	0.0141407	1.0102316	0.1075097
10 MeV	0.2157556	0.0001206	0.0217701	0

As a measure of neutron and photon fluxes we plotted the ratio of activities while using regular and heavy water moderators (see Figure 22 and Figure 23). As expected, the ratio of the activities of ^{196}Au using D_2O and H_2O is close to one for lower energies and drops for higher energies as the on-axis and off-axis photons have different energy spectra. The ratio of the activities of ^{198}Au using D_2O and H_2O is also predictable being very high for low energies and getting close to unity for lower energies.

The results of the activation were compared to the MCNPX prediction of the yields and found to be in good agreement. Figure 24 and Figure 25 show both predicted and measured yields of Au-196 indirectly confirming photon flux simulations. Similarly, Figure 27 and Figure 26 show both predicted and measured yields of Mn-56 indirectly confirming neutron flux simulations. There is a discrepancy between the simulated and measured values, which can be explained by the lack of reliable cross-section and electron beam misalignment during the experiments. Taking all the sources of uncertainty into account, we find the agreement between our yield predictions and measurements to be satisfactory.

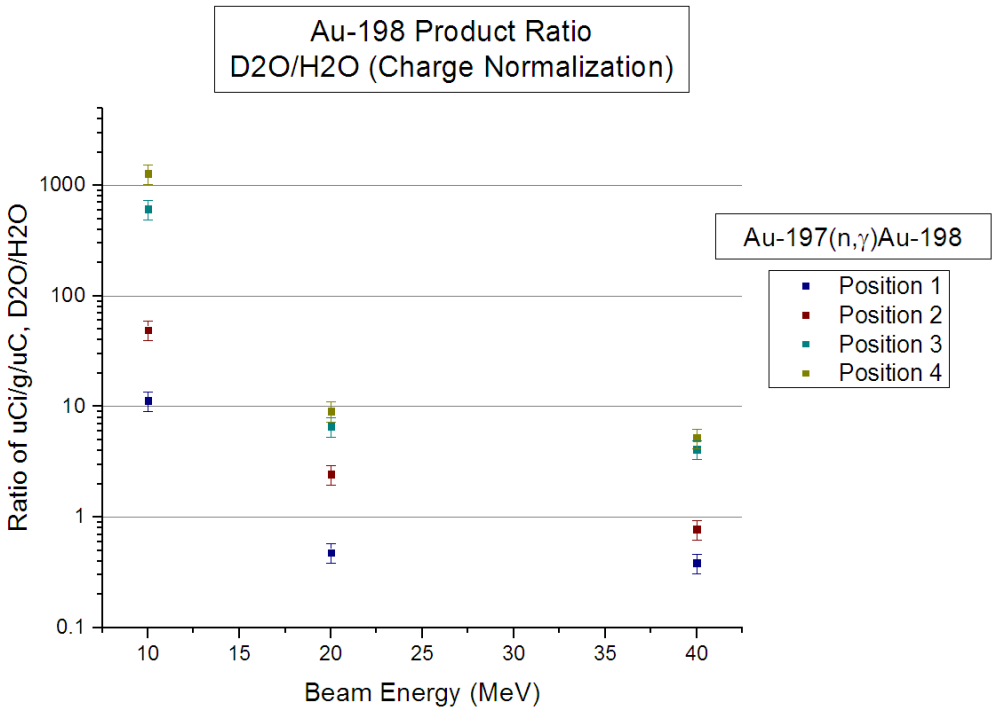

Figure 22. A measure of neutron flux shown by the ratio of activities while using water and heavy water moderators.

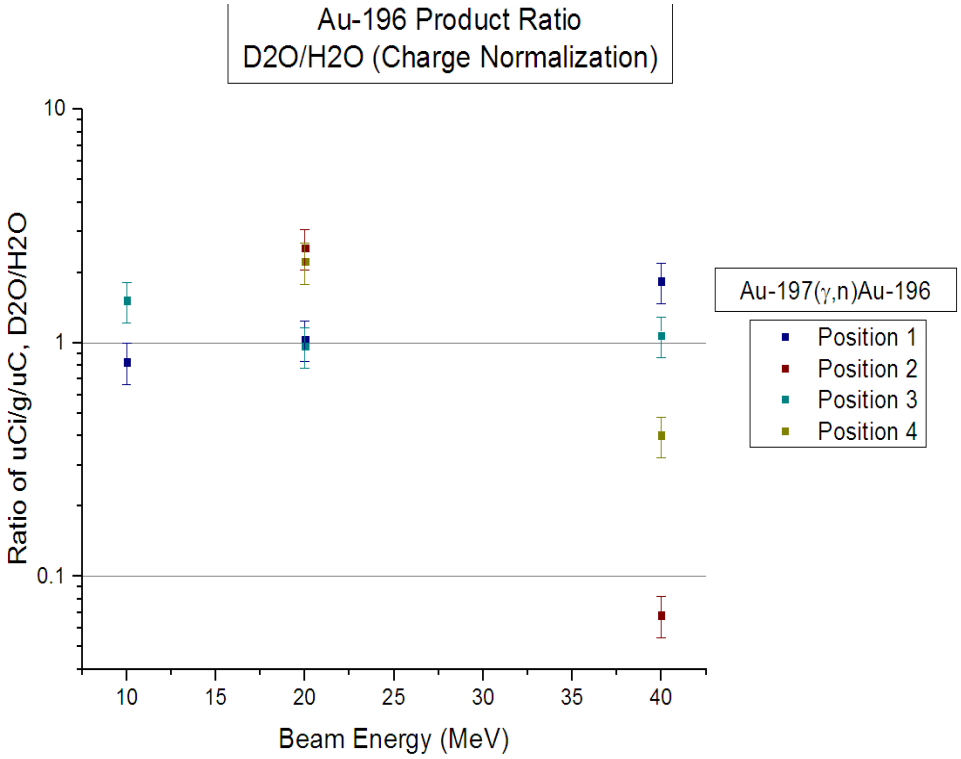

Figure 23. A measure of photon flux shown by the ratio of activities while using water and heavy water moderators.

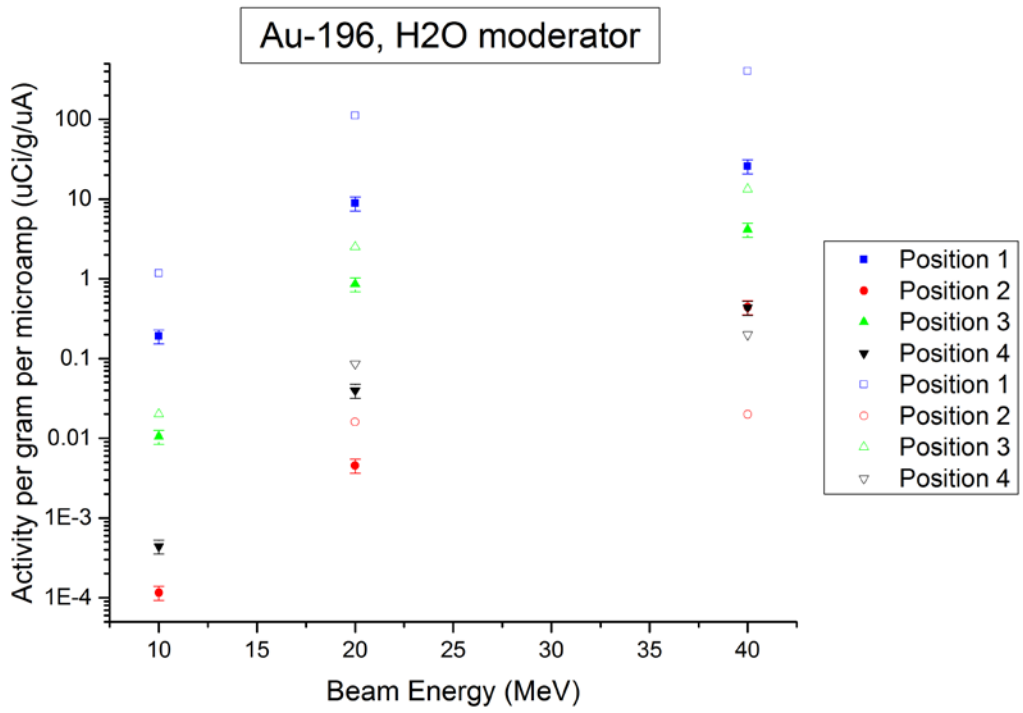

Figure 24. Comparison of MNCPX predicted (empty symbols) and measured (filled symbols) Au-196 yields using H_2O as moderator.

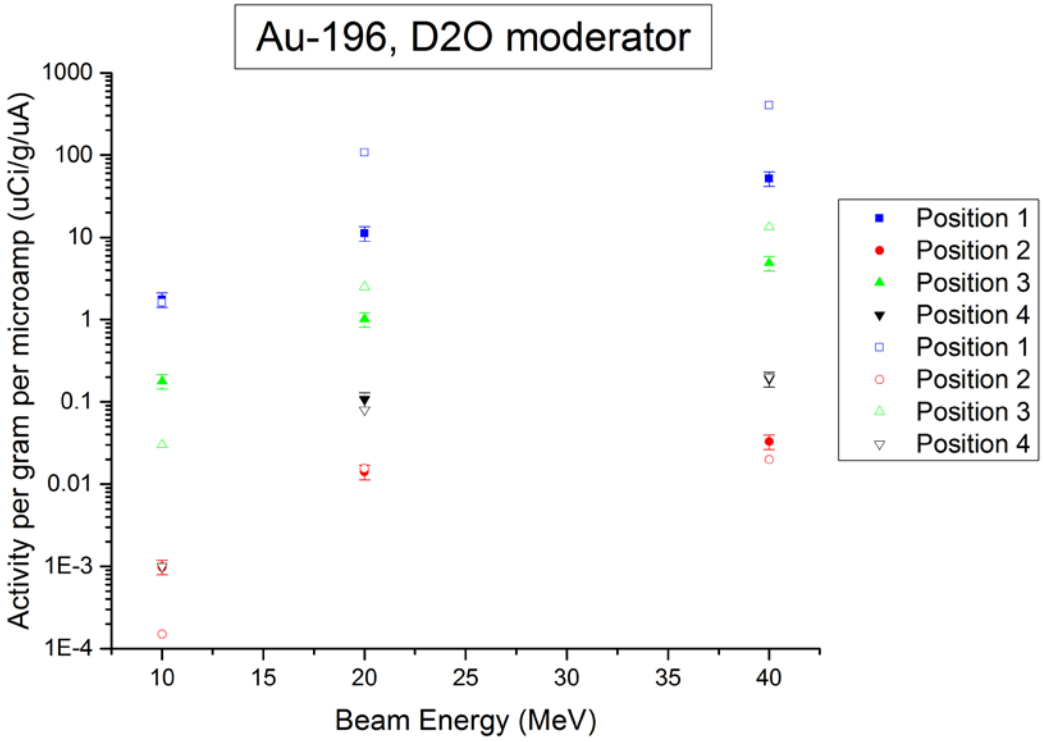

Figure 25. Comparison of MNCPX predicted (empty symbols) and measured (filled symbols) Au-196 yields using D_2O as moderator.

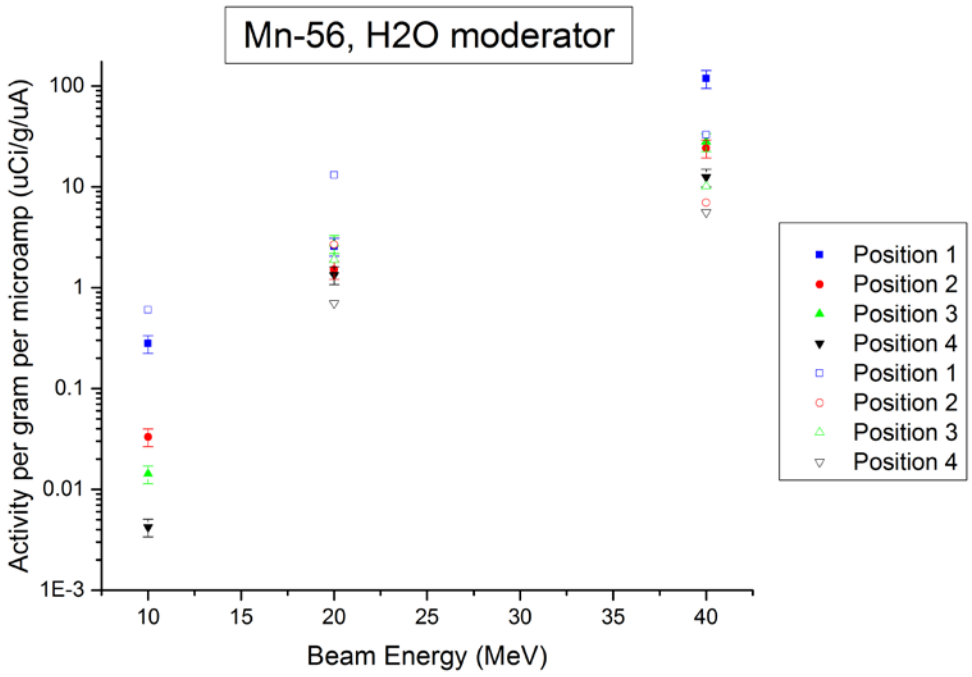

Figure 26. Comparison of MNCPX predicted (empty symbols) and measured (filled symbols) Mn-56 yields using H_2O as moderator.

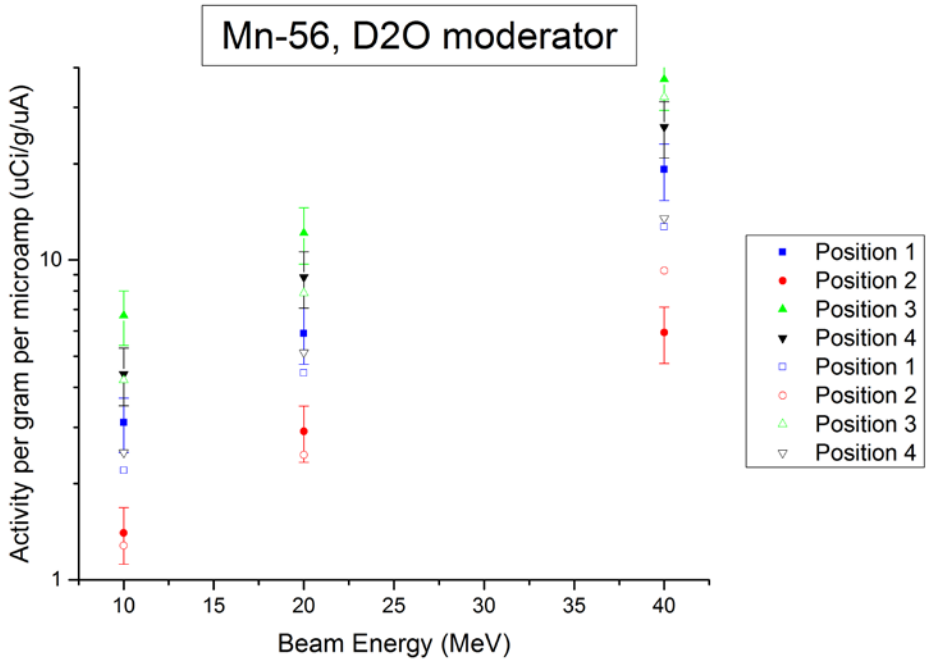

Figure 27. Comparison of MNCPX predicted (empty symbols) and measured (filled symbols) Mn-56 yields using D_2O as moderator.

NEW FACILITY AND LICENSING

To produce medical and industrial isotopes with the 40 MeV, 100 kW superconducting linac, a facility had to be developed. Once the general parameters were determined for the superconducting linac, a facility design including the power, cryogenics, and support facilities had to be developed. The facility and accelerator licensing considerations were determined so a "blueprint" for a complete radioisotope production facility could be replicated at sites around the country. This SBIR project did not fund any construction of equipment or facilities, and did not develop production methods for specific radioisotopes.

Using the "blueprint" developed under the 2013 SBIR, Niowave moved ahead with construction of a radioisotope production facility. This new production facility now houses a superconducting linac and associated equipment, and is sited at the nearby Lansing International Airport. Niowave is currently licensed by the State of Michigan to operate superconducting linacs up to 40 MeV and 100 kW at both the headquarters and airport facilities. The airport facility has a similar footprint to the Niowave Electron Research and Development center adjacent to the headquarters. Niowave plans to begin produce initial quantities of radioisotopes in 2015. The radioisotopes will be produced by a number of photonuclear reactions, including photo-proton, photo-neutron, neutron capture and photofission.

Figure 28. New facility being built near Lansing International Airport (shown in October 2014). The building was completed in early 2015 and is currently being outfitted with equipment. The initial linac license has been received from the State of Michigan, and initial production is expected by the end of 2015

We have received approval of the shielding plan for electron beams up to 40 MeV and 100 kW at the Airport Facility from the state's department of Licensing and Regulatory Affairs (LARA) radiation safety section. The license to operate the first superconducting linac at the airport facility has been received by LARA.

Niowave has received two licenses from the NRC. The first license allows us to possess, machine, and transport source material (natural uranium, depleted uranium, and natural thorium). The second license allows for possession of low enriched uranium (LEU), and also allows for production of small (R&D) quantities of radioisotopes from stable targets, and from uranium fission. The State of Michigan and NRC licenses allow Niowave to conduct R&D work on isotope production using superconducting electron linacs.

PARTNERSHIPS

Lastly, during the course of this SBIR, Niowave has established close partnership with several radioisotope distributors and radioactive source producers. These include Lantheus Medical Imaging, a leading distributor of ^{99m}Tc; ISOFLEX, the premier global distributor of stable and radioactive isotopes for science, medicine and industry; and Source Production & Equipment Co., Inc., a leading supplier of industrial gamma radiography equipment, specializing in ^{192}Iridium, ^{75}Se and ^{60}Co devices and sources. In addition to the radioisotope partnerships, Niowave has also established working relationships with commercial LEU suppliers. Establishing these relationships and obtaining the required licenses has positioned Niowave to become a leading domestic producer of medical and industrial isotopes.

REFERENCES

[1] Meeting Isotope Needs and Capturing Opportunities for the Future: The 2015 Long Range Plan for the DOE-NP Isotope Program, NSAC Isotopes Subcommittee, July 20, 2015

[2] Public Law 112-239, The National Defense Authorization Act of 2013, includes Section 3171, American Medical Isotope Production Act, signed into law January 2, 2013.

[3] Danon Y. et al., 2008. Medical isotope production using A 60 MeV linear electron accelerator, NS transactions,2008 ANS National Meeting, Anaheim, CA, vol. 98, 894-89510

[4] Maslov, O.D. et al., 2006. Preparation of ^{225}Ac by ^{226}Ra(γ,n) photonuclear reaction on an electron accelerator, MT-25 Microtron., *Radiochemistry*, 48, 195197

[5] Starovoitova, V.N. et al., 2014. Production of medical radioisotopes with linear accelerators. *Appl.Radiat. Isot.*. 85:39-44

[6] Danon Y. et al., 2008. Medical isotope production using A 60 MeV linear electron accelerator, NS transactions,2008 ANS National Meeting, Anaheim, CA, vol. 98, 894-89510

[7] Maslov, O.D. et al., 2006. Preparation of ^{225}Ac by ^{226}Ra(γ,n) photonuclear reaction on an electron accelerator, MT-25 Microtron., *Radiochemistry*, 48, 195197

[8] Starovoitova, V.N. et al., 2014. Production of medical radioisotopes with linear accelerators. *Appl.Radiat. Isot.*. 85:39-44

[9] Handbook on Lead-bismuth Eutectic Alloy and Lead Properties, Materials Compatibility, Thermal-hydraulics and Technologies, OECD/NEA Nuclear Science Committee, Working Party on Scientific Issues of the fuel Cycle, Working Group on Lead-bismuth Eutectic, 2007